THE JOURNAL OF BIOLOGICAL CHEMISTRY
© 1993 by The American Society for Biochemistry and Molecular Biology, Inc.

Vol. 268, No. 31, Issue of November 5, pp. 22984-22991, 1993
Printed in U.S.A.

Comparison of the Membrane Binding Kinetics of Bovine Prothrombin and Its Fragment 1*

(Received for publication, March 1, 1993, and in revised form, June 8, 1993)

Kenneth H. Pearce‡, Martin Hof§¶, Barry R. Lentz§‖, and Nancy L. Thompson‡‖

From the Departments of ‡Chemistry and §Biochemistry & Biophysics, University of North Carolina, Chapel Hill, North Carolina 27599

Total internal reflection fluorescence microscopy has been used to compare the membrane binding characteristics of fluorescein-labeled bovine prothrombin and fluorescein-labeled bovine prothrombin fragment 1. The Ca^{2+}-dependent association of these proteins with quartz-supported planar membranes composed of mixtures of phosphatidylserine (2–10 mol %) and phosphatidylcholine was examined. Equilibrium binding measurements showed that the apparent equilibrium dissociation constants increased with decreasing molar fractions of phosphatidylserine and that the dissociation constants were somewhat lower for intact prothrombin. Kinetic measurements, using fluorescence photobleaching recovery, showed that the measured dissociation rates were approximately equivalent for prothrombin and fragment 1 and did not change with the protein solution concentration or the molar fraction of phosphatidylserine. The kinetic data also implied that the surface binding mechanism for both proteins is more complex than a simple reversible reaction between monovalent proteins and monovalent surface sites. Measured equilibrium and kinetic constants are reported and compared for prothrombin and fragment 1 on planar membranes.

The conversion of prothrombin to thrombin is a crucial step in thrombosis and hemostasis. This proteolytic step is catalyzed by a membrane-bound enzyme (factor X_a) in the presence of a membrane-bound cofactor (factor V_a), calcium ions, and a phospholipid surface (1–3). Efficient membrane binding of prothrombin as well as catalysis by the prothrombinase enzyme complex requires negatively charged phospholipids such as phosphatidylserine (4–7). The fragment 1 portion of the proenzyme is thought to be primarily responsible for the association of prothrombin with the membrane and the subsequent membrane-mediated catalysis to thrombin by factor X_a. The binding event is believed to occur through a mechanism in which the interaction of Ca^{2+} with γ-carboxyglutamic acid residues in prothrombin facilitates association with membranes containing acidic lipids (8).

The membrane-localized assembly and activation of the prothrombinase enzyme complex and subsequent prothrombin cleavage involves an interplay between chemical reaction processes (protein-protein interactions and protein-membrane interactions) and transport processes (lateral diffusion, rotational diffusion, and segmental flexibility both in solution and on the membrane) (9). Understanding the manner in which these reaction and transport processes are coupled at the membrane surface requires physical (*e.g.* spectroscopic) measurements. Characterizing these processes will also serve as a paradigm for other Ca^{2+}-mediated enzymatic functions in blood coagulation that require the association of proteins containing γ-carboxyglutamic acid residues with membranes that contain negatively charged phospholipids.

One method for obtaining quantitative information about the physical dynamics of proteins at membrane surfaces is to use substrate-supported planar membranes and techniques in fluorescence microscopy (10–13). In previous studies, total internal reflection fluorescence microscopy (TIRFM)[1] (14) has been used to examine the equilibrium binding of bovine prothrombin and its fragment 1 to supported membranes composed of mixtures of phosphatidylcholine and phosphatidylserine (15, 16). These studies showed that the proteins bound to the planar membranes in a Ca^{2+}-specific manner and that the equilibrium dissociation constants were approximately equivalent to those measured on phospholipid vesicles by more conventional methods.

Total internal reflection illumination has also been combined with fluorescence photobleaching recovery (TIR-FPR) (14, 17) to examine the binding kinetics of bovine prothrombin fragment 1 at the planar membranes (16). However, the TIR-FPR data were complicated by two factors. First, the TIR-FPR recovery curves were partially diffusion-controlled at low protein solution concentrations, so that the intrinsic surface dissociation kinetic rates could not be determined at physiological concentrations. Second, for high protein concentrations where the TIR-FPR recovery curves were reaction-limited, the data were not monoexponential; whether this characteristic arose from an intrinsically complex surface binding mechanism or from lateral protein-protein interactions resulting from nonphysiologically high protein surface densities was unclear.

In the work herein, the molar fraction of phosphatidylserine in the planar membranes has been decreased in that a previous theory (18) predicts that TIR-FPR recovery curves should be more reaction-controlled when the equilibrium dissociation

* This work was supported by National Science Foundation Grant DMB-9024028 (to N. L. T), United States Public Health Service Grant HL-45916 (to B. R. L.), National Institutes of Health Grant HL-20161 (to R. G. H), and by a Graduate Fellowship from the Hercules Corp. (to K. H. P.) The costs of publication of this article were defrayed in part by the payment of page charges. This article must therefore be hereby marked "*advertisement*" in accordance with 18 U.S.C. Section 1734 solely to indicate this fact.

¶ Present address: Institut für Physikalische Chemie, Universität Würzburg, 8700 Würzburg, Germany.

‖ To whom correspondence should be addressed.

[1] The abbreviations used are: TIRFM, total internal reflection fluorescence microscopy; POPC, 1-palmitoyl-2-oleoyl-3-*sn*-phosphatidylcholine; PS, bovine brain phosphatidylserine; TIR-FPR, total internal reflection fluorescence photobleaching recovery; TBS, Tris-buffered saline.

constant is higher or the surface density of bound proteins is lower. Therefore, one purpose of the present investigation was to measure membrane binding kinetics for both prothrombin and fragment 1 at lower surface densities in an attempt to reveal mechanistic information concerning the mode of membrane binding for vitamin K-dependent proteins.

MATERIALS AND METHODS

Proteins—Prothrombin was obtained from bovine plasma and fragment 1 was produced and purified as previously described (19–21). Both proteins were greater than 95% pure as determined by high performance liquid chromatography on Mono Q (prothrombin) and sodium dodecyl sulfate-polyacrylamide gel electrophoresis (prothrombin and fragment 1). Protein concentrations were determined by ultraviolet spectrophotometry at 280 nm (prothrombin, ϵ = 1.44 ml mg^{-1} cm^{-1}, molecular mass = 72 kDa; fragment 1, ϵ = 1.05 ml mg^{-1} cm^{-1}, molecular mass = 23 kDa). Prothrombin and fragment 1 were conjugated with fluorescein 5-isothiocyanate (Molecular Probes, Eugene, OR) as described (15). The concentrations of labeled proteins were determined by the bicinchonic acid assay (Pierce Chemical Co.) and the molar ratios of fluorescein to protein (0.6–1.6) were determined using the molar absorptivity of protein-conjugated fluorescein at 494 nm (ϵ = 64,800 M^{-1} cm^{-1}; Molecular Probes). Protein solutions were stored in Tris-buffered saline (TBS; 0.05 M Tris, 0.1 M NaCl, pH 7.4). Prothrombin was used within 48 h following final purification by high performance liquid chromatography on Mono Q (Pharmacia LKB Biotechnology Inc.) and fragment 1 was stored at −70 °C until immediately before use.

Planar Membranes—Supported planar membranes were deposited on 1 × 1 inch fused silica substrates as previously described (15, 16). Small unilamellar vesicles were prepared at 2 mM from 1-palmitoyl-2-oleoyl-3-*sn*-phosphatidylcholine (POPC) and bovine brain phosphatidylserine (PS) (Avanti Polar Lipids) by sonication and air ultracentrifugation. Vesicles were fused and deposited on the substrates by spontaneous adsorption for 25 min followed by rinsing with 2 ml of TBS. Planar membranes were then treated with 200 μl of 20 mg/ml bovine serum albumin (Sigma) to block nonspecific binding sites, rinsed with 2 ml of TBS, and treated with 250 μl of TBS containing various concentrations of unlabeled protein, fluorescein-labeled protein, 10 mM Ca_2Cl or 1 mM Na_2EDTA, and 2 mg/ml bovine serum albumin. Samples containing protein were prepared so that labeled protein was diluted 5–10-fold by unlabeled protein to yield the appropriate final protein concentration. All 250-μl samples were incubated at room temperature for at least 30 min prior to use.

Fluorescence Microscopy and Data Analysis—The fluorescence microscope for TIRFM was as previously described (16, 22, 23), with two modifications. First, the 488-nm argon ion laser beam was passed through a 488-nm interference filter. Second, the laser beam was directed through two lenses to reduce the beam diameter; the focal lengths were 223 and 25 mm and the lenses were separated by approximately 248 mm. This arrangement produced an elliptically shaped evanescent wave with minor and major axes approximately equal to 15 and 120 μm, respectively. Parameters for TIRFM and TIR-FPR were as follows: fused silica prism, 1 cm^3; incidence angle, 75°; objective (Nikon), water, 40 ×, 0.75 N.A.; focal length of auxiliary lens, 50 mm; evanescent wave depth, ~820 Å; bleaching time, 10 ms −1 s; depth of bleach, 30–95%; observation beam power, 0.1–5 microwatts; bleaching beam power, 20–100 milliwatts. For measurements with circularly polarized excitation light, a quarter-wave plate (Melles-Griot, Irvine, CA) was introduced into the path of the laser beam.

TIRFM equilibrium binding curves and TIR-FPR recovery curves were fit to theoretical forms with the iterative Gauss-Newton nonlinear curve fitting routine in the ASYST software package (Macmillan Software, New York). For TIR-FPR recovery curves, the experimental data were fit to monoexponential and biexponential forms by minimizing a chi-squared statistic that was weighted according to the photon noise. The chi-squared values for the best fits to different functional forms were compared with an *F*-statistic (24).

RESULTS

Equilibrium Binding of Prothrombin and Fragment 1 to Planar Membranes—TIRFM was used to measure the surface-associated fluorescence on PS/POPC planar membranes that had been treated with solutions of fluorescein-labeled prothrombin or fluorescein-labeled fragment 1. The evanescently excited fluorescence on PS/POPC planar membranes was significantly higher when the solutions contained Ca^{2+} rather than EDTA (Fig. 1). Also, in the presence of Ca^{2+}, the measured fluorescence was saturable with increasing prothrombin or fragment 1 solution concentrations, whereas, with EDTA, the fluorescence was approximately linear with the protein concentration. These results confirm that both prothrombin and its fragment 1 were binding to the membranes in the physiologically relevant, Ca^{2+}-specific and PS-specific manner.

The equilibrium binding data shown in Fig. 1 were fit to the following approximate functional form, which describes a reversible bimolecular reaction between monovalent proteins and monovalent surface sites.

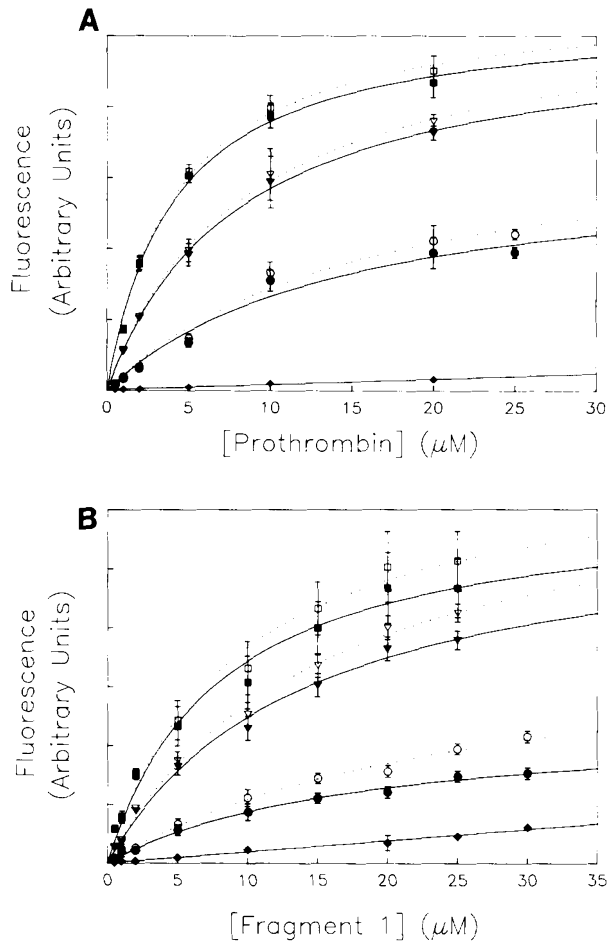

FIG. 1. **Equilibrium binding of prothrombin and fragment 1 to planar membranes.** Binding curves were constructed by measuring the evanescently excited fluorescence of (*a*) prothrombin or (*b*) fragment 1 on various PS/POPC planar membranes as a function of the protein solution concentration. Binding curves were measured for membranes with 2 mol % PS (*circles*), 6 mol % PS (*triangles*), and 10 mol % PS (*squares*). All samples contained 10 mM Ca^{2+} except for the control samples which contained 1 mM EDTA (*diamonds*). The 1 mM EDTA curve is the average of data for 2, 6, and 10 mol % PS membranes. Each point is the average of two binding curves obtained from independent vesicle and protein preparations. Uncertainties are displayed as standard deviations. Theoretical curves were generated by fitting the directly measured fluorescence values (*open symbols, dotted lines*) and the corrected fluorescence values (*closed symbols, solid lines*) to Equation 1 (see Table I).

TABLE I

Equilibrium binding of prothrombin and fragment 1 to planar membranes

The equilibrium binding data shown in Fig. 1 were curve-fit to Equation 1 to obtain best fit values of the equilibrium dissociation constants, K_d, and the theoretical maximum relative fluorescence values, $F(\infty)$. The equilibrium binding data for prothrombin and fragment 1 on PS/POPC planar membranes in the presence of Ca^{2+} were analyzed by two methods. In one method, the fraction of the measured fluorescence due to solution fluorescence (excited by the finite depth of the evanescent field) and nonspecifically bound protein was assumed to be negligible; *i.e.* no background was subtracted. In the other method, the amount of the measured fluorescence that was due to background was assumed to equal the fluorescence measured on the same type of planar membrane and for the same solution concentration of protein, but in the presence of EDTA. For this analysis, the fluorescence values for samples with EDTA were subtracted as background from the fluorescence values for samples with Ca^{2+}. The best fit values of K_d and $F(\infty)$ were assumed to vary more for identical data sets and different types of background subtraction than for binding curves obtained with independent protein and vesicle preparations and the same type of background subtraction. Therefore, the apparent values of K_d and $F(\infty)$ were taken to equal the averages of the two values obtained from the data as analyzed with or without background substration, and uncertainties in the average values were taken to equal one-half of the difference of the two values. The surface site-densities were calculated as described in the text using Equation 2. For membranes with 2 mol % PS, data were measurable only for concentrations approximately equal to twice the measured value of K_d. Therefore, values are given as lower or upper limits.

	K_d	$F(\infty)$	[N]	$[N]^{-1}$
mol % PS	*μM*	*relative*	*molecules/μm²*	*Å²/molecule*
Prothrombin				
2	≥15.1 ± 0.7	≥0.64 ± 0.08	≥17,000 ± 2200	≤5900 ± 800
6	8.2 ± 0.2	0.98 ± 0.04	24,100 ± 3200	4100 ± 500
10	4.2 ± 0.1	1.00 ± 0.02	39,200 ± 5500	2600 ± 400
Fragment 1[2]				
2	≥21.8 ± 4.0	≥0.48 ± 0.23	≥18,200 ± 2700	≤5500 ± 800
6	14.6 ± 0.8	0.98 ± 0.08	19,400 ± 2000	5200 ± 500
10	8.5 ± 0.6	1.00 ± 0.06	27,500 ± 3800	3600 ± 500

$$F([A]) = \frac{F(\infty)[A]}{K_d + [A]} \qquad \text{(Eq. 1)}$$

In this analysis, the protein solution concentration, $[A]$, and the surface fluorescence, $F([A])$, were known parameters; and the dissociation constant, K_d, and the fluorescence at infinite protein solution concentration, $F(\infty)$, were free parameters. The measured dissociation constants for both prothrombin and fragment 1 were in the μM range (Table I),[2] increased with decreasing molar fractions of PS, and were smaller for prothrombin than for fragment 1. For both proteins, the best fit values of $F(\infty)$ were approximately equivalent for membranes with 6 or 10 mol % PS and were consistent with the lower limits measured for membranes with 2 mol % PS (Table I). Because the measured fluorescence for a given surface density of prothrombin was not necessarily equal to the measured fluorescence for the same surface density of fragment 1, the values of $F(\infty)$ for prothrombin and fragment 1 are not directly comparable.

Surface site densities, $[N]$, were estimated by measuring the fraction of the evanescently excited fluorescence that was bleachable (25) and using the expression,

$$[N] \approx d(K_d + [A]_{sat}) \frac{F(+)}{F(-)} \frac{B(+)}{1 - B(-)} \qquad \text{(Eq. 2)}$$

where $[A]_{sat}$ is a protein solution concentration that (nearly) saturates the surface sites; d (≈820 Å) is the evanescent field depth; $F(+)$ and $F(-)$ are the measured fluorescence intensities in the presence and absence of Ca^{2+}, respectively; and $B(+)$ and $B(-)$ are the fractions of the measured fluorescence that were bleachable in the presence and absence of Ca^{2+}, respectively.[3] The absolute surface site densities determined from these data using Equation 2 (Table I) increased for both fragment 1 and prothrombin with PS content. Prothrombin packed more densely on the planar membranes compared to fragment 1.

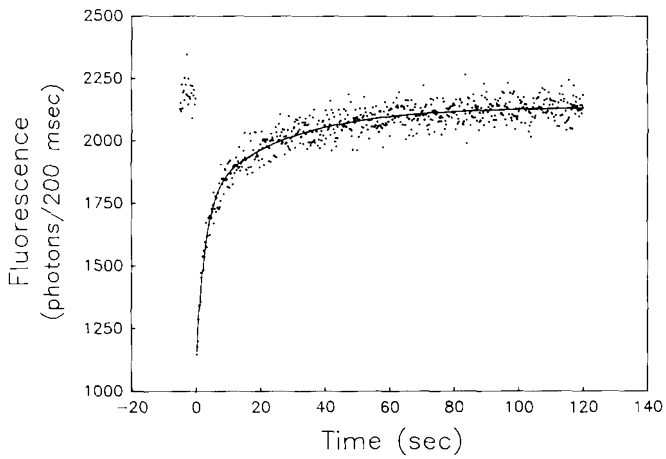

FIG. 2. **Representative TIR-FPR fluorescence recovery curve.** Shown is a typical recovery curve for 1 μM prothrombin with 10 mM Ca^{2+} on a 6 mol % PS planar membrane. The *line* shows the best fit to Equation 3 with $n = 2$.

Surface Binding Kinetics of Prothrombin and Fragment 1—TIR-FPR was used to examine the surface binding kinetics of prothrombin and fragment 1 at PS/POPC planar membranes. As shown in Fig. 2, the characteristic time for fluorescence recovery was on the order of seconds and nearly complete recovery occurred after a few minutes.

[2] The K_d values for fragment 1 differ somewhat from those given in a previous publication (16). This discrepancy is due to the additional measurements of fluorescence at higher solution concentrations (25 and 30 μM). Analysis by Equation 1 of the data shown in Fig. 1*b* in which only points up to 10 μM were used yielded dissociation constants similar to those previously reported. Because data were obtained closer to saturation in the present study, the reported dissociation constants are more accurate than those given previously.

[3] The measured values of $F(+)/F(-)$, $B(+)$ and $B(-)$ were as follows: 25 μM fragment 1, 10 mol % PS, 11.1, 0.90, 0.40; 25 μM fragment 1, 6 mol % PS, 9.2, 0.70, 0.35; 25 μM fragment 1, 2 mol % PS, 4.2, 0.75, 0.60; 20 μM prothrombin, 10 mol % PS, 27.0, 0.85, 0.30; 20 μM prothrombin, 6 mol % PS, 22.7, 0.61, 0.20; 25 μM prothrombin, 2 mol % PS, 8.6, 0.75, 0.25.

TIR-FPR recovery curves were fit to the following empirical form,

$$F(t) = F(-) - \left[a_0 + \sum_{i=1}^{n} a_i e^{-k_i t}\right] \quad \text{(Eq. 3)}$$

where a_i (for $i = 0$ to n) and k_i (for $i = 1$ to n) were free parameters and $n = 1$ or $n = 2$. The fractional recovery associated with each rate was calculated by dividing the amplitudes a_i by the sum of all amplitudes,

$$r_i = \frac{a_i}{\sum_{i=0}^{n} a_i} \quad \text{(Eq. 4)}$$

for $i = 1$ to n. The average recovery rate, k_{ave}, was calculated as the following.

$$k_{ave} = \frac{r_1 k_1 + r_2 k_2}{r_1 + r_2} \quad \text{(Eq. 5)}$$

Analysis with an F-statistic of the chi-squared goodness-of-fit parameters was used to determine if a statistically significant, better fit was obtained for $n = 2$ (five free parameters) relative to $n = 1$ (three free parameters); a better fit yields a value of $F > 3$ (24). The values of F ranged from 50 to 300 (for all sample types) and were therefore much larger than the critical value of 3. Therefore, all TIR-FPR data were fit to Equation 3 with $n = 2$.[4]

The four measured parameters (k_1, k_2, r_1, and r_2) and the value of k_{ave}, obtained from the best fits of the TIR-FPR data to Equation 3 with $n = 2$, were approximately equivalent for most samples (Tables II and III).

Several control measurements were performed. First, in the absence of the bleach pulse, the fluorescence was constant for at least 5 min. Second, the best fit values of k_1, k_2, r_1, and r_2 did not change significantly when the duration of the bleach pulse was varied from 10 ms to 1 s; when data were obtained by repetitively bleaching the same area (up to five sequential curves); or when the incident laser beam was circularly rather than linearly polarized. Therefore, both photoinduced artifacts such as chemical cross-linking (26) and fluorescence emission or collection artifacts (14) are unlikely.

[4] For most samples, fluorescence recovery was monitored with sample times equal to 200 ms and for 120 s after the photobleaching pulse. For data with 200-ms sample intervals but longer durations (500 s), the best fit values of k_i were slightly reduced (2.0-fold). For curves with a postbleach duration of 120 s but with a sample interval of 50 ms, the values of k_i and r_i were increased (1.4- and 1.1-fold, respectively). Data obtained with a 10-ms sample interval and a shorter postbleach duration (30 s) yielded larger k_i values (~5-fold) and slightly reduced r_i values (1.2-fold). To determine whether these trends resulted from a property intrinsic to the data or from a curve fitting artifact, a set of theoretical, biexponential recovery curves ($k_1 = 0.5$, $k_2 = 0.025$, $r_1 = 0.5$, $r_2 = 0.3$) were generated by using Equation 3 and adding Gaussian noise. The best fit values of the rates and amplitudes for these simulated recovery curves were very close to the (known) theoretical values for all four analysis conditions (50-ms sample interval, 120 s duration; 200-ms sample interval, 500 s duration; 200-ms sample interval, 120 s duration; 10-ms sample interval, 30 s duration). Therefore, the anomalous behavior of the best fit parameters in the analysis of the true TIR-FPR data arose from a property intrinsic to the data, perhaps because the data were not completely described by a sum of two exponential terms. In a previous work that examined the binding kinetics of fragment 1 on planar membranes (16), it was shown that the best fits of TIR-FPR recovery curves to Equation 3 with $n = 2$ (five free parameters) or $n = 3$ (seven free parameters) had values of F that were approximately equal to 4; therefore, whether or not the fits with three exponentials were statistically better than the fits with two exponentials was inconclusive.

DISCUSSION

Equilibrium Binding as Measured by TIRFM—TIRFM was used to measure the apparent equilibrium dissociation constants for prothrombin and fragment 1 on PS/POPC planar membranes (Table I). The measured dissociation constants display the well-known trend that the K_d values become smaller with increasing molar fractions of PS (5, 7, 27). The absolute K_d values for membranes containing 10 mol % PS compare favorably with literature values determined for prothrombin on small, unilamellar vesicles by quasielastic light scattering (5, 7).

Surface Dissociation Kinetics as Measured by TIR-FPR—A previous theoretical work has predicted the shapes of TIR-FPR recovery curves for the case in which soluble ligands bind to discrete surface sites through a simple bimolecular reversible reaction (18). The general expression reflects a rather complex coupling between surface dissociation kinetics, solution diffusion, and surface diffusion. There are four characteristic rates whose values determine the rate and shape of fluorescence recovery. One rate is the average intrinsic dissociation constant, k_{off}. The other three rates describe diffusion in solution or on the membrane and are given by,

$$R_N = \frac{D_{soln}(K_d + [A])^2}{[N]^2} \quad \text{(Eq. 6)}$$

$$R_{L,S} = \frac{D_{soln,surf}}{s^2} \quad \text{(Eq. 7)}$$

In Equations 6 and 7, D_{soln} and D_{surf} are the protein diffusion coefficients in solution and on the surface, respectively, and s is the semiminor axis of the elliptically shaped evanescent illumination. R_N is the rate for diffusion in solution through a distance equal to the ratio of the surface density of bound ligand and the solution concentration of free ligand. R_L and R_S are the rates for diffusion in solution and on the surface, respectively, through the evanescently illuminated area.

In the absence of surface diffusion, surface dissociation (k_{off}) and solution diffusion (R_N and R_L) act approximately in series; *i.e.* the slower of the two processes dominates the rate of fluorescence recovery. Also, R_N and R_L correspond (roughly) to diffusion in solution in directions perpendicular and parallel to the surface, respectively, so that the diffusional process with the larger rate will be the dominant mode of replacing bleached, surface-bound ligands. Surface diffusion acts approximately in parallel with the binding/dissociation kinetics, so that the faster of those two processes governs the rate of fluorescence recovery. Thus, the observed rate of fluorescence recovery will be approximately given by the following.

$$k_{ave} \approx \max[R_S, \min\{k_{off}, \max(R_L, R_N)\}] \quad \text{(Eq. 8)}$$

For large observation areas, $R_S \rightarrow 0$. Then, in the "diffusion limit" of TIR-FPR, $k_{ave} \approx R_N$ and the recovery rate increases with the protein solution concentration (16). In the "reaction limit," $k_{ave} \approx k_{off}$, and the recovery rate does not depend on the bulk protein concentration and provides information about the kinetics of the intrinsic surface dissociation process. For a simple surface binding mechanism that occurs between monovalent proteins and monovalent surface sites, the shape of the reaction-limited recovery curve is predicted to be a single exponential with a rate equal to the surface dissociation rate constant, *i.e.* Equation 3 with $n = r_1 = 1$ (18).

In a previous work with planar membranes containing 25 mol % PS, concentration-independent (*i.e.* reaction-limited) recovery rates were found only at fragment 1 concentrations

TABLE II

Dissociation rates and fractional recoveries for prothrombin

Values were obtained from the best fits of TIR-FPR recovery curves to Equation 3 with $n = 2$, and are the averages of 3–13 measured curves. Average recovery rates, k_{ave}, were determined for individual recovery curves using Equation 5. Errors are standard deviations.

PS	[A]	k_1	r_1	k_2	r_2	$r_1 + r_2$	k_{ave}
mol %	*μM*	s^{-1}	*× 100*	s^{-1}		*× 100*	s^{-1}
2	1	0.54 ± 0.17	34 ± 6	0.023 ± 0.006	29 ± 1	64 ± 6	0.30 ± 0.12
	2	0.49 ± 0.22	36 ± 5	0.022 ± 0.003	36 ± 3	72 ± 5	0.26 ± 0.12
	5	0.48 ± 0.10	33 ± 2	0.023 ± 0.001	43 ± 3	76 ± 2	0.22 ± 0.05
	10	0.65 ± 0.40	26 ± 4	0.021 ± 0.004	42 ± 6	68 ± 5	0.27 ± 0.19
	20	0.53 ± 0.25	31 ± 8	0.019 ± 0.004	38 ± 9	69 ± 11	0.26 ± 0.17
6	1	0.32 ± 0.07	55 ± 7	0.032 ± 0.007	35 ± 3	90 ± 5	0.21 ± 0.05
	2	0.36 ± 0.14	52 ± 3	0.024 ± 0.013	33 ± 6	85 ± 7	0.23 ± 0.08
	10	0.44 ± 0.18	33 ± 3	0.019 ± 0.003	36 ± 1	68 ± 3	0.22 ± 0.10
10	1	0.27 ± 0.10	49 ± 4	0.032 ± 0.006	39 ± 5	87 ± 4	0.17 ± 0.06
	2	0.35 ± 0.02	44 ± 3	0.025 ± 0.003	39 ± 4	83 ± 3	0.20 ± 0.02
	10	0.63 ± 0.09	35 ± 2	0.024 ± 0.001	31 ± 3	66 ± 2	0.34 ± 0.05

TABLE III

Dissociation rates and fractional recoveries for fragment 1

Values were obtained from the best fits of TIR-FPR recovery curves to Equation 3 with $n = 2$, and are the averages of 3–13 curves. Average recovery rates, k_{ave}, were determined for individual recovery curves using Equation 5. Errors are standard deviations.

PS	[A]	k_1	r_1	k_2	r_2	$r_1 + r_2$	k_{ave}
mol %	*μM*	s^{-1}	*× 100*	s^{-1}		*× 100*	s^{-1}
2	0.5	0.59 ± 0.29	26 ± 2	0.030 ± 0.005	38 ± 3	64 ± 3	0.26 ± 0.12
	1	0.46 ± 0.14	31 ± 3	0.027 ± 0.003	45 ± 6	76 ± 5	0.21 ± 0.08
	5	0.70 ± 0.25	29 ± 3	0.021 ± 0.004	49 ± 6	78 ± 7	0.28 ± 0.11
	20	0.43 ± 0.14	28 ± 13	0.022 ± 0.002	47 ± 11	75 ± 10	0.18 ± 0.10
6	0.5	0.32 ± 0.09	45 ± 6	0.029 ± 0.005	40 ± 4	85 ± 6	0.18 ± 0.05
	1	0.49 ± 0.23	41 ± 3	0.025 ± 0.006	35 ± 2	76 ± 2	0.27 ± 0.12
	5	0.40 ± 0.03	38 ± 2	0.025 ± 0.001	44 ± 3	82 ± 4	0.20 ± 0.02
	20	0.46 ± 0.16	39 ± 15	0.023 ± 0.009	42 ± 3	81 ± 5	0.23 ± 0.11
10	0.5	0.41 ± 0.22	40 ± 6	0.032 ± 0.012	45 ± 3	84 ± 4	0.20 ± 0.08
	1	0.37 ± 0.18	38 ± 1	0.023 ± 0.005	48 ± 6	86 ± 7	0.18 ± 0.09
	5	0.40 ± 0.15	37 ± 3	0.022 ± 0.004	41 ± 2	79 ± 2	0.20 ± 0.07
	20	0.38 ± 0.16	36 ± 12	0.019 ± 0.006	41 ± 8	77 ± 9	0.20 ± 0.13

that were greater than 10 μM and not physiologically relevant (16). The primary motivation for the present investigation was to examine the membrane binding kinetics of fragment 1 and prothrombin using planar membranes, TIR-FPR, and low, physiological solution concentrations of protein. According to previous theoretical predictions (18), the transition between diffusion-limited and reaction-limited systems depends on the surface site density and equilibrium dissociation constant; decreasing the former or increasing the latter optimizes the probability that TIR-FPR data will be reaction-limited and reflect true surface dissociation kinetic rates. In this study, lower surface concentrations of acidic lipids have been used to accommodate reaction-limited kinetics.

The values of the three characteristic rates shown in Equations 6 and 7 may be estimated as follows. The maximum surface diffusion coefficient of the bound protein is (probably) the phospholipid diffusion coefficient, or $D_{surf} \leq 10^{-8}$ cm^2/s, and $s \approx 7.5$ μm, so that $R_S \leq 0.02$ s^{-1}. Also, because $D_{soln} \approx 5 \times 10^{-7}$ cm^2/s, $R_L \approx 0.9$ s^{-1} (Fig. 3). The predicted values of R_N may be calculated from Equation 6 and the information in Table I, and are shown in Fig. 3. For prothrombin, the calculated values of R_N range from 0.3 to 77 s^{-1}; for fragment 1, the R_N values range from 2 to 95 s^{-1}.

Because R_S is much slower than the observed recovery rate, k_{ave}, the fluorescence recovery curves are not affected by surface diffusion (Equation 8). In addition, for all but the lowest solution concentrations of prothrombin on membranes with 10 mol % PS, the values of R_N are larger than the value of R_L, so that replenishment of bleached, surface-bound molecules occurs primarily through transport in a direction perpendicular rather than parallel to the surface. By comparing the data in Tables II and III with the calculations shown in Fig. 3, one may note that (for most samples) k_{ave} is much less than the larger of R_N and R_L so that the TIR-FPR recovery curves are "reaction-limited" and the measured recovery rates primarily reflect the true rates of surface dissociation (see Equation 8). This conclusion is consistent with the result that the measured values of k_{ave} do not depend on the protein solution concentration, which would suggest the dominance of R_N (Equation 6). Therefore, for most samples, one may conclude that the measured values of k_{ave} are true kinetic dissociation rates, which we denote by k_{off}. Because one possible natural substrate for prothrombin binding in the human blood coagulation system has been shown to be platelet membrane vesicles (28–30) that have a PS content of about 10 mol % (31), the measured intrinsic dissociation rates of fragment 1 and prothrombin offer a reasonable model for these interactions on native-like membranes at a physiologically relevant protein concentration.

Apparent Kinetic Dissociation and Association Rate Constants—The apparent dissociation rate for both prothrombin and fragment 1 on planar membranes with low molar fractions

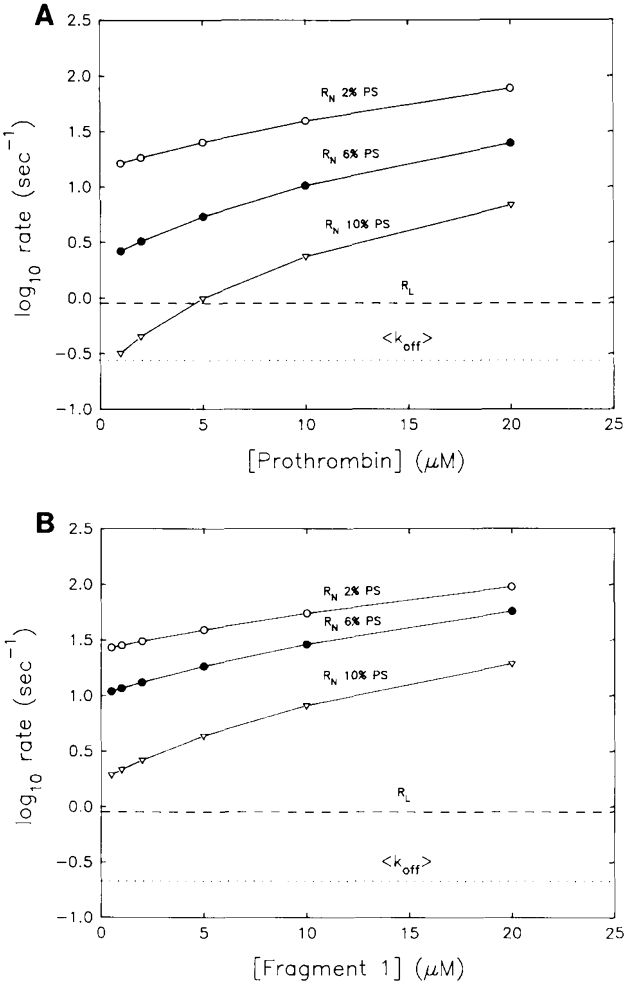

FIG. 3. **Characteristic rates.** Values for the rates R_N and R_L were calculated for different membrane types using Equations 6 and 7. The value shown for <k_{off}> is an average dissociation rate for all membrane types (Table IV).

of PS (2–10 mol %) was, within experimental uncertainty, independent of the protein type (prothrombin or fragment 1), the protein solution concentration, and the molar fraction of PS. This measured value for $\langle k_{off} \rangle$ is approximately equivalent to the dissociation rate previously measured by TIR-FPR for high concentrations of fragment 1 (>10 μM) on 25 mol % PS planar membranes (16). However, the measured value of $\langle k_{off} \rangle$ is approximately an order of magnitude smaller than a previous measure for prothrombin on small, unilamellar vesicles of the same PS content (3 s^{-1}) obtained using light scattering methods (32).

Average association rates $\langle k_{on} \rangle$ were determined using the measured values of $\langle k_{off} \rangle$, K_d, and the following expression.

$$\langle k_{on} \rangle = \frac{\langle k_{off} \rangle}{K_d} \qquad \text{(Eq. 9)}$$

Because the values of $\langle k_{off} \rangle$ did not significantly depend on the PS content and the values of K_d decreased with increasing PS content, it followed that the values of $\langle k_{on} \rangle$ increased with increasing PS content (Table IV).

The values for $\langle k_{on} \rangle$ (~10^4-10^5 M^{-1} s^{-1}) are considerably lower than the on-rate previously measured for prothrombin on PS/POPC small, unilamellar vesicles by light scattering (≈10^7 M^{-1} s^{-1}) (32). However, similarly low on-rates have also recently been measured for other proteins at planar or cell

TABLE IV

Average intrinsic dissociation/association rates for prothrombin and fragment 1

Average dissociation rates were calculated using reaction-limited TIR-FPR data for fragment 1 (all solution concentrations) and prothrombin (all solution concentrations for 2 and 6% PS membranes and 10 μM for 10% PS membranes) (Tables II and III). The dissociation rate values, <k_{off}>, are the means of k_{ave} calculated for individual recovery curves using Equation 5. Average association rates were determined using Equation 9. Values are averages of 5–29 trials for prothrombin and 34–42 trials for fragment 1. Uncertainties are standard errors in the means. Comparison of the <k_{off}> values for 2 and 10 mol % PS membranes using a two-tailed, unpaired t test yielded p values of 0.19 for prothrombin and 0.048 for fragment 1. The p values comparing <k_{on}> measurements with 2 and 10 mol % PS membranes were <<0.0001 for prothrombin and fragment 1.

PS	$\langle k_{off} \rangle$	$\langle k_{on} \rangle \times 10^{-4}$
mol %	s^{-1}	M^{-1} s^{-1}
Prothrombin		
2	0.26 ± 0.03	≤1.7 ± 0.2
6	0.22 ± 0.02	2.7 ± 0.2
10	0.34 ± 0.02	8.1 ± 0.5
Fragment 1		
2	0.25 ± 0.02	≤1.1 ± 0.1
6	0.20 ± 0.01	1.4 ± 0.1
10	0.19 ± 0.02	2.2 ± 0.2

surfaces (17, 33). The discrepancy between the apparent kinetic rate constants measured by TIR-FPR and light scattering suggests that membrane curvature may play a role in determining the stability of protein-membrane complexes. Significant differences in the apparent bimolecular rate constant for the conversion of prothrombin to thrombin by phospholipid-bound prothrombinase complexes on vesicles and planar membranes have also been reported (34). In addition, the Ca^{2+}-dependent lipid binding properties of annexin V are highly dependent on vesicle curvature (35) and the dissociation rate of factor V_a light chain from highly curved, small, unilamellar vesicles is slower than that from less curved, large unilamellar vesicles (36). Other possible explanations for the discrepancy between the values of $\langle k_{off} \rangle$ and $\langle k_{on} \rangle$ shown in Table IV and the previously measured values on vesicles (32) include crowding, rebinding, orientational, and electrostatic effects (see below).

Both estimates of $\langle k_{on} \rangle$ are much lower than the apparent second order rate constants (k_{cat}/K_m) reported for prothrombin activation to thrombin by the fully assembled prothrombinase on phospholipid vesicles (37). There are at least three possible explanations for this seeming anomaly. 1) If the primary substrate for the prothrombinase complex is prothrombin in solution, then the membrane binding rate for prothrombin would not be directly related to the rate of thrombin formation. 2) If the primary substrate is membrane-bound prothrombin, then the rate of thrombin formation will be determined not only by the rate of membrane binding, but also by the rates of lateral diffusion on the surface and dissociation. These factors do not couple in such a way that the value of k_{cat}/K_m is always less than the value of $\langle k_{on} \rangle$ (calculations not shown). 3) Because of the difference between prothrombin binding rates observed for vesicles and planar membranes, it may not be accurate to directly compare binding rates obtained on planar membranes with enzymatic rates obtained on vesicles.

Comparison of Apparent Rate Constants for Prothrombin and Fragment 1—For each membrane composition, intact prothrombin bound to planar membranes with a slightly higher affinity than did fragment 1, confirming a similar

observation for planar membranes containing 30 mol % PS (15). Because the values of $\langle k_{off} \rangle$ were approximately equivalent for prothrombin and fragment 1, the values of $\langle k_{on} \rangle$ were somewhat larger for prothrombin. Possible explanations for this observation include the following: 1) prothrombin, but not fragment 1, experiences a weak, Ca^{2+}-independent interaction with PS/POPC and perhaps POPC membranes (15, 21); 2) prothrombin experiences domain reorganizations and changes in interdomain interactions in its non-fragment 1 portion when bound to PS-containing membranes (38, 39); 3) an unidentified interaction, such as a long-range electrostatic force (40), between the whole prothrombin molecule and the membrane surface alters the protein orientation relative to the membrane surface so that the PS-specific sites in the fragment 1 region are more readily occupied by membrane-associated PS.

Complex Dissociation Kinetics for Prothrombin and Fragment 1—Even for the low PS densities explored in this work, the reaction-limited TIR-FPR recovery curves for both fragment 1 and prothrombin were not well described by a single exponential shape (Fig. 2).[4] This result implies that the association of fragment 1 and prothrombin with PS/POPC membranes proceeds through a mechanism that is more complex than a discrete, reversible, bimolecular reaction between monovalent ligands and surface sites. Earlier studies of the membrane binding kinetics of fragment 1 (16), prothrombin (32), and factor X (41) have also implied that, at least at high protein concentrations, the binding process is complex and multiphasic. It is possible that the nature of protein-membrane interactions, in general, is intrinsically complex and cannot be adequately described by conventional kinetics (42, 43).

Although the specific reasons for the complex binding behavior are not known, there are several possible explanations that may be grouped into the following four categories.

1) The existence of multiple protein species in solution (for example, protein dimers) might result in complex membrane-binding behavior as observed by TIR-FPR. Solution-phase dimerization of both prothrombin and prothrombin fragment 1 have been described previously (44, 45). However, the low protein solution concentrations used in the current study makes solution-phase dimer formation an unlikely contributor to our results. In addition, significant amounts of impurities in the prothrombin and fragment 1 preparations are not present (15, 16). Finally, it is unlikely that heterogeneity in the labeled proteins is responsible for the non-monoexponential TIR-FPR data, in that statistically equivalent results were obtained for both proteins and for several different protein preparations with different fluorophore-to-protein ratios. Also, equivalent results were obtained for fragment 1 labeled either with fluorescein isothiocyanate or with nitrobenzoxadiazole fluoride (data not shown).

2) The non-monoexponential TIR-FPR recovery could also be explained, in general, by the existence of different types of surface binding sites. However, this possibility is considered to be unlikely in that the equilibrium binding data (Fig. 1; see Ref. 16) are described well with a single dissociation constant.

3) The existence of more than one membrane-bound protein species could result in non-monoexponential TIR-FPR recovery curves (16, 17). Although bovine prothrombin is known to undergo conformational changes when bound to PS-containing membranes (38, 39), these changes have been observed only for intact prothrombin and not for fragment 1. Thus, the previously observed membrane-induced conformational changes are an unlikely explanation for the observed non-monoexponential recovery curves in that the TIR-FPR data are identical for prothrombin and fragment 1. Another possible explanation for multiple membrane-bound protein species is the formation of protein dimers on the membrane surface. However, for this possible phenomenon to explain the data, the dimerization constant would have to be approximately equivalent for both prothrombin and fragment 1, which seems unlikely. A third explanation for the existence of different membrane-bound species is that the proteins bind to the membranes through a multi-step binding process in which a weak, initial interaction is followed by a relatively slow rearrangement leading to mass-action controlled occupation of specific sites on prothrombin by membrane-associated PS (7). A fourth explanation for the existence of different membrane-bound species is that both prothrombin and fragment 1 can be bound to PS/POPC membrane surfaces through direct interactions with different numbers of PS molecules or calcium ions. For this mechanism, the TIR-FPR rates would reflect interconversion between, and/or release from, different membrane-bound states.

4) In general, the observed complex recovery curves may reflect an unanticipated feature of the general mechanism of extrinsic protein binding to planar membrane surfaces (*e.g.* crowding, orientational, rebinding, or electrostatic effects). Strong geometric effects on binding kinetic rates have recently been experimentally demonstrated for Fab-hapten kinetics (46). In addition, biexponential or even more complex recovery curves have been observed in all previous TIR-FPR measurements of biologically specific protein-membrane kinetics (16, 17, 33).[5]

Acknowledgments—We gratefully acknowledge Drs. Richard G. Hiskey and Lee G. Pedersen for helpful conversations and critical review of the manuscript.

REFERENCES

1. Jackson, C. M., and Nemerson, Y. (1980) *Annu. Rev. Biochem.* **49,** 765–811
2. Nesheim, M. E., Hubbard, L. S., Tracy, P. B., Bloom, J. W., Myrmel, K. H., and Mann, K. G. (1980) in *The Regulation of Coagulation*, pp. 145–149, Elsevier/North-Holland, Amsterdam
3. Mann, K. G., Nesheim, M. E., Church, W. R., Haley P., and Krishnaswamy, S.(1990) *Blood* **76,** 1–16
4. Bangham, A. D. (1961) *Nature* **192,** 1197–1198
5. Nelsestuen, G. L., and Broderius, M. (1977) *Biochemistry* **16,** 4172–4177
6. Jones, M. E., Lentz, B. R., Dombrose, F. A., and Sandberg, H. (1985) *Thromb. Res.* **39,** 711–724
7. Cutsforth, G. A., Whitaker, R. N., Hermans, J., and Lentz B. R. (1989) *Biochemistry* **28,** 7453–7459
8. Dombrose, F. A., Gitel, S. N., Zawalich, K., and Jackson, C. M. (1979) *J. Biol. Chem.* **254,** 5027–5040
9. Abbott, A. J., and Nelsestuen, G. L. (1988) *FASEB J.* **2,** 2858–2866
10. McConnell, H. M., Watts, T. H., Weis, R. M., and Brian, A. A. (1986) *Biochim Biophys. Acta* **864,** 95–106
11. Thompson, N. L., and Palmer, A. G. (1988) *Comm. Mol. Cell. Biophys.* **5,** 39–56
12. Thompson, N. L., Palmer, A. G., Wright, L. L., and Scarborough, P. E. (1988) *Comm. Mol. Cell. Biophys.* **5,** 109–131
13. Liebmann, L. W., Robinson, J. A., and Mann, K. G. (1991) *Rev. Sci. Instrum.* **62,** 2083–2092
14. Axelrod, D., Hellen, E. H., and Fulbright, R. M. (1992) in *Topics in Fluorescence Spectroscopy* (Lakowicz, J. R., ed) Vol. 3, pp. 289–341, Plenum Press, New York
15. Tendian, S. W., Lentz, B. R., and Thompson, N. L. (1991) *Biochemistry* **30,** 10991–10999
16. Pearce, K. H., Hiskey, R. G., and Thompson, N. L. (1992) *Biochemistry* **31,** 5983–5995
17. Pisarchick, M. L., Gesty, D., and Thompson, N. L. (1992) *Biophys. J.* **63,** 215–223
18. Thompson, N. L., Burghardt, T. P., and Axelrod, D. (1981) *Biophys. J.* **33,** 435–454
19. Mann, K. G. (1977) *Methods Enzymol.* **45,** 123–156
20. Pollock, J. S., Shepard, A. J., Weber, D. J., Olson, D. L., Klapper, D., Pedersen, L., and Hiskey, R. G. (1988) *J. Biol. Chem.* **263,** 14216–14223
21. Tendian, S. W., and Lentz, B. R. (1990) *Biochemistry* **29,** 6720–6729
22. Pisarchick, M. L., and Thompson, N. L. (1990) *Biophys. J.* **58,** 1235–1249
23. Poglitsch, C. L., and Thompson, N. L. (1990) *Biochemistry* **29,** 248–254

[5] H. V. Hsieh and N. L. Thompson, manuscript in preparation.

24. Wright, L. L., Palmer, A. G., and Thompson, N. L. (1988) *Biophys. J.* **54,** 463–470
25. Schmidt, C. F., Zimmerman, R. F., and Gaub, H. (1990) *Biophys. J.* **57,** 577–588
26. Sheetz, M. P., and Koppel, D. E. (1979) *Proc. Natl. Acad Sci. U. S. A.* **76,** 3314–3317
27. Kop, J. M. M., Cuypers, P. A., Lindhout, T., Hemker, H. C., and Hermens, W. T. (1984) *J. Biol. Chem.* **259,** 13993–13998
28. Sandberg, H., Bode, A. P., Dombrose, F. A., and Lentz, B. R. (1985) *Thromb. Res.* **39,** 63–79
29. Bode, A. P., Sandberg, H., Dombrose, F. A., and Lentz, B. R. (1985) *Thromb. Res.* **39,** 49–61
30. Sims, P. J., Faioni, E. L., Wiedmer, T., and Shattil, S. J. (1988) *J. Biol. Chem.* **263,** 18205–18212
31. Sandberg, H., Andersson, L.-O., and Höglund, S. (1982) *Biochem. J.* **203,** 303–311
32. Wei, G. J., Bloomfield, V. A., Resnick, R. M., and Nelsestuen, G. L.(1982) *Biochemistry* **21,** 1949–1959
33. Hellen, E. H., and Axelrod, D. (1991) *J. Fluoresc.* **1,** 113–128
34. Giesen, P. L., Willems, G. M., and Hermens, W. Th. (1991) *J. Biol. Chem.* **266,** 1379–1382
35. Andree, H. A. M., Stuart, M. C. A., Hermens, W. Th., Reutelingsperger, C. P. M., Hemker, H. C., Frederik, P. M., and Willems, G. M. (1992) *J. Biol. Chem.* **267,** 17907–17912
36. Abbott, A. J., and Nelsestuen, G. L. (1987) *Biochemistry* **26,** 7994–8003
37. Pei, G., Powers, D. D., and Lentz, B. R. (1993) *J. Biol. Chem.* **268,** 3226–3233
38. Wu, J. R., and Lentz, B. R. (1991) *Biophys. J.* **60,** 70–80
39. Lentz, B. R., Wu, J. R., Sorrentino, A. M., and Carleton, J. N. (1991) *Biophys. J.* **60,** 942–951
40. Soriano-Garcia, M., Padmanabhan, K., de Vos, A. M., and Tulinsky, A. (1991) *Biochemistry* **31,** 2554–2566
41. Krishnaswamy, S., Jones, K. C., and Mann, K. G. (1988) *J. Biol. Chem.* **263,** 3823–3834
42. Steinbach, P. J., Chu, K., Frauenfelder, H., Johnson, J. B., Lamb, D. C., Niehaus, G. U., Sauke, T. B., and Young, R. D. (1992) *Biophys. J.* **61,** 235–245
43. Nagle, J. F. (1992) *Biophys. J.* **63,** 366–370
44. Tarvers, R. C., Noyes, C. M., Tarvers, J. K., and Lundblad, R. L. (1986) *J. Biol. Chem.* **261,** 4855–4859
45. Jackson, C. M., Brenckle, G. M., Hogg, P. J., and Winzor, D. J. (1987) *J. Biol. Chem.* **262,** 13472–13475
46. Schweitzer-Stenner, R., Licht, A., and Pecht, I. (1992) *Biophys. J.* **63,** 551–562